DISCLAIMER

This report was prepared as an account of work sponsored by an agency of the United States Government. Neither the United States Government nor any agency thereof, nor any of their employees, makes any warranty, express or implied, or assumes any legal liability or responsibility for the accuracy, completeness, or usefulness of any information, apparatus, product, or process disclosed, or represents that its use would not infringe privately owned rights. Reference herein to any specific commercial product, process, or service by trade name, trademark, manufacturer, or otherwise does not necessarily constitute or imply its endorsement, recommendation, or favoring by the United States Government or any agency thereof. The views and opinions of authors expressed herein do not necessarily state or reflect those of the United States Government or any agency thereof. Reference herein to any social initiative (including but not limited to Diversity, Equity, and Inclusion (DEI); Community Benefits Plans (CBP); Justice 40; etc.) is made by the Author independent of any current requirement by the United States Government and does not constitute or imply endorsement, recommendation, or support by the United States Government or any agency thereof.

ORNL/TM-2025/4007

BOILER Experiment Material Characterization and HFIR Irradiation Status

Nick Russell
Yukinori Yamamoto
Tim Graening
Timothy Lach
Marie Romedenne
Janelle Wharry
Kory Linton

September 2025

OAK RIDGE National Laboratory

ORNL IS MANAGED BY UT-BATTELLE LLC FOR THE US DEPARTMENT OF ENERGY

ORNL/TM-2025/4007

Nuclear Energy and Fuel Cycle Division

BOILER EXPERIMENT MATERIAL CHARACTERIZATION AND HFIR IRRADIATION STATUS

Nick Russell
Yukinori Yamamoto
Tim Graening
Timothy Lach
Marie Romedenne
Janelle Wharry
Kory Linton

DOE-NE Nuclear Science User Facility (NSUF)
Milestone M3UF-25OR021003012

September 2025

Prepared by
OAK RIDGE NATIONAL LABORATORY
Oak Ridge, TN 37831
managed by
UT-BATTELLE LLC
for the
US DEPARTMENT OF ENERGY
under contract DE-AC05-00OR22725

CONTENTS

LIST OF FIGURES

ACKNOWLEDGMENTS

This research is supported by the US Department of Energy (DOE), Office of Nuclear Energy, Nuclear Science User Facilities (NSUF) program. The specimen alloys referenced in this report were fabricated in support of the Advanced Fuels Campaign within the Fuel Cycle Research and Development program, Office of Nuclear Energy. The report was authored by UT-Battelle under Contract No. DE-AC05-00OR22725 with the US DOE.

1. INTRODUCTION

Pre-oxidized alumina-forming austenitic (AFA) steels have been previously identified [1] as candidate alloys for structural components in lead-cooled fast reactors (LFRs). They offer compatibility with liquid Pb, high-temperature strength, formability, and cost advantages. However, variations in Ni content can affect the formation and stability of the Al_2O_3 layer, influencing compatibility with liquid Pb [2]. The effect of fast neutron irradiation on Al_2O_3 stability in liquid Pb also requires evaluation. Therefore, understanding how Ni concentrations impacts pre-oxidized AFAs under combined extremes of irradiation and liquid metal corrosion is essential before safe deployment.

The Behavior Of In-situ Lead Environments & Radiation (BOILER) experiment was developed under the Nuclear Science User Facilities (NSUF) program to integrate alloy development, irradiation experiment design, and irradiated materials characterization. In this effort, two pre-oxidized AFA steels with 20 wt% and 25 wt% Ni, hereinafter referred to as GA05-20Ni and GA05-25Ni, were produced [1]. An irradiation experiment was then planned for the High Flux Isotope Reactor (HFIR), designed for passive heating of irradiation rabbit capsules from gamma heating in the HFIR flux trap (1×10^{15} n/cm^2·s, >0.1 MeV). This heating melts Pb and exposes the pre-oxidized AFA steel specimens to nominal temperatures of 400 and 650°C. Detailed neutronics and thermal analyses were performed, though based on nominal design rather than as-built, as-irradiated conditions.

This report documents further characterization of the pre-oxidized AFAs in the unirradiated condition. It also includes as-built thermal analysis using measured component dimensions, updated fill gas concentrations, and actual HFIR irradiation positions. Finally, the report summarizes capsule fabrication, current irradiation status, projected completion, estimated damage accumulation, and initial plans for post-irradiation examination plans.

2. SPECIMEN MATERIALS CHARACTERIZATION

2.1 MICROSTRUCTURE CHARACTERIZATION

Crystallographic orientation distributions of both Ni variant alloys were measured via electron backscatter diffraction (SEM-EBSD) using a Quanta 650 FEG scanning electron microscope equipped with an EDAX detector. The instrument was operated at 25 kV accelerating voltage, 2 µm step size, and 4×4 detector binning for data acquisition. Inverse pole figure (IPF) maps were generated with MTEX software for visualization. Maps were taken from regions with equiaxed, homogeneous grains (excluding elongated grain regions near plate surfaces). No dominant grain texture was observed in either alloy, as shown in Figure 1. GA05-25Ni exhibited a larger average grain size and broader distribution (95 ± 22 µm) compared to GA05-20Ni (64 ± 12 µm).

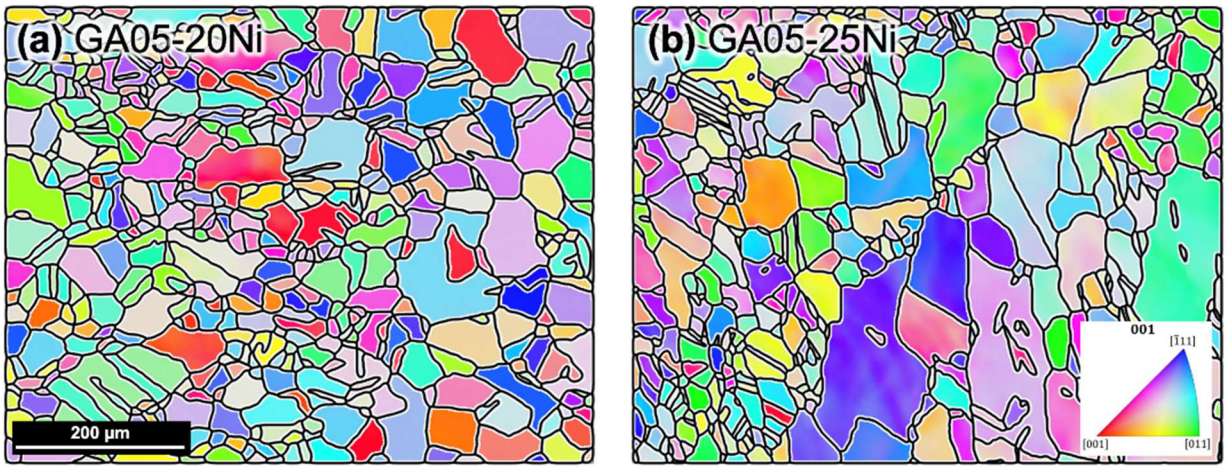

Figure 1. IPF color maps of (a) GA05-20Ni and (b) GA05-25Ni showing the crystallographic orientation distribution of grains acquired by SEM-EBSD.

To evaluate Al_2O_3 scale stability under fast neutron flux (1×10^{15} n/cm^2·s, >0.1 MeV), high temperature (450 and 650 °C), and liquid lead exposure (99.999 at.% metallic purity), all SS-J3 tensile specimens were pre-oxidized in air at 800 °C for 2 h in a Carbolite box furnace. To limit thermal transients on the established oxide layer nature, the specimens were inserted once the furnace reached 800 °C rather than gradually heated. Samples were pre-oxidized in two batches (batch 1 and batch 2) under identical conditions. After oxidation, specimens from both batches were selected for baseline room temperature tensile and surface hardness measurements. Batch1 samples were used in the HFIR experiment, while batch 2 was reserved non-irradiated analysis.

The oxide layers were characterized by transmission electron microscopy (TEM) before HFIR exposure. TEM specimens were prepared using a Thermo Fisher Scientific Helios 5 Hydra plasma focused ion beam / scanning electron microscope (FIB/SEM) with 30 kV Xe^+ ions for initial thinning followed by 5 kV and 2 kV final polishing. Microstructural and elemental mapping was performed on a Thermo Fisher Scientific Talos F200X TEM/scanning TEM (STEM) equipped with the SuperX 4-sector energy-dispersive x-ray spectroscopy (EDS) system, a high-resolution Ceta camera, STEM bright field (BF) detector, and three STEM annular dark field (ADF) detectors operated in both TEM and STEM mode. This enabled identification of structural defects, elemental segregation, and nanoscale precipitates. The TEM and STEM-EDS analyses were performed using the Thermo Fisher Velox software.

Figure 2(a) and Figure 2(b) present BF TEM images and underfocus BF TEM image maps of the near surface area and the Al_2O_3 layer on the surface of the batch 1 versions of GA05-20Ni and GA05-25Ni, respectively. Underfocus images revealed nanoscale cavities in the Al_2O_3 layer prior to HFIR exposure (Figure 2c, d). The oxide scale thickness was thicker for the GA05-25Ni (294 ± 30 nm) than for the GA05-20Ni (103 ± 10 nm). Al_2O_3 growth also led to subsurface dissolution of Al-rich precipitates, consistent with prior reports [3, 4, 5]. This dissolution region was thicker in the GA05-25Ni specimen (3.0 ± 0.6 µm) than in the GA05-20Ni specimen (1.7 ± 0.4 µm).

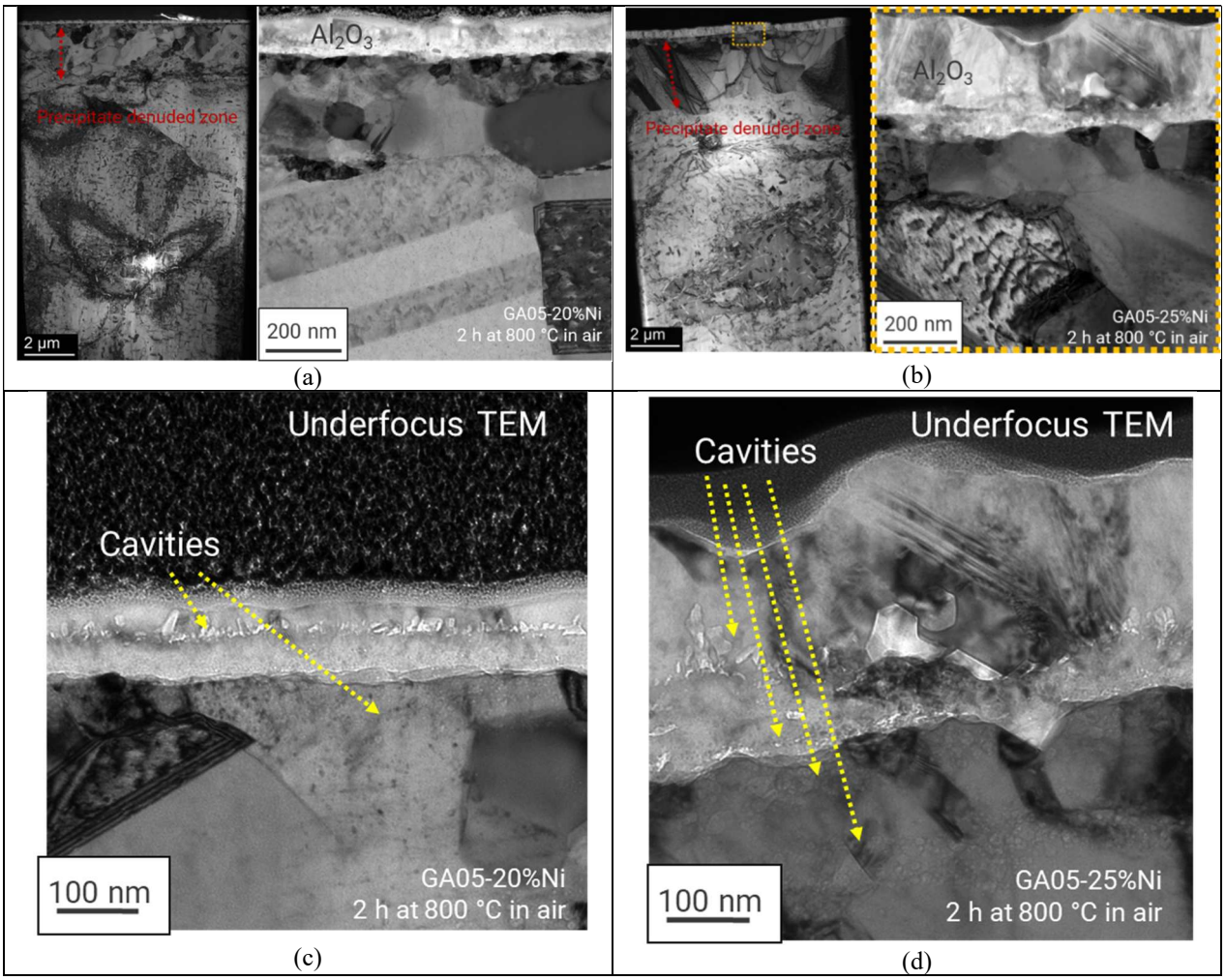

Figure 2. TEM BF (a, b) and TEM underfocus (c, d) images of Al_2O_3 layer formed on the surface of GA05-20Ni and GA05-25Ni after 2 h oxidation in air at 800 °C.

In the case of GA05-25Ni, a mostly Al-rich oxide (Al_2O_3) formed, with Fe- and Mn-rich regions and an Al- and Cr-rich interlayer (Figure 3b). In the case of GA05-20Ni the Al- and Cr-rich interlayer was also present, but an additional outer Fe- and Al-rich oxide layer was observed (Figure 3a).

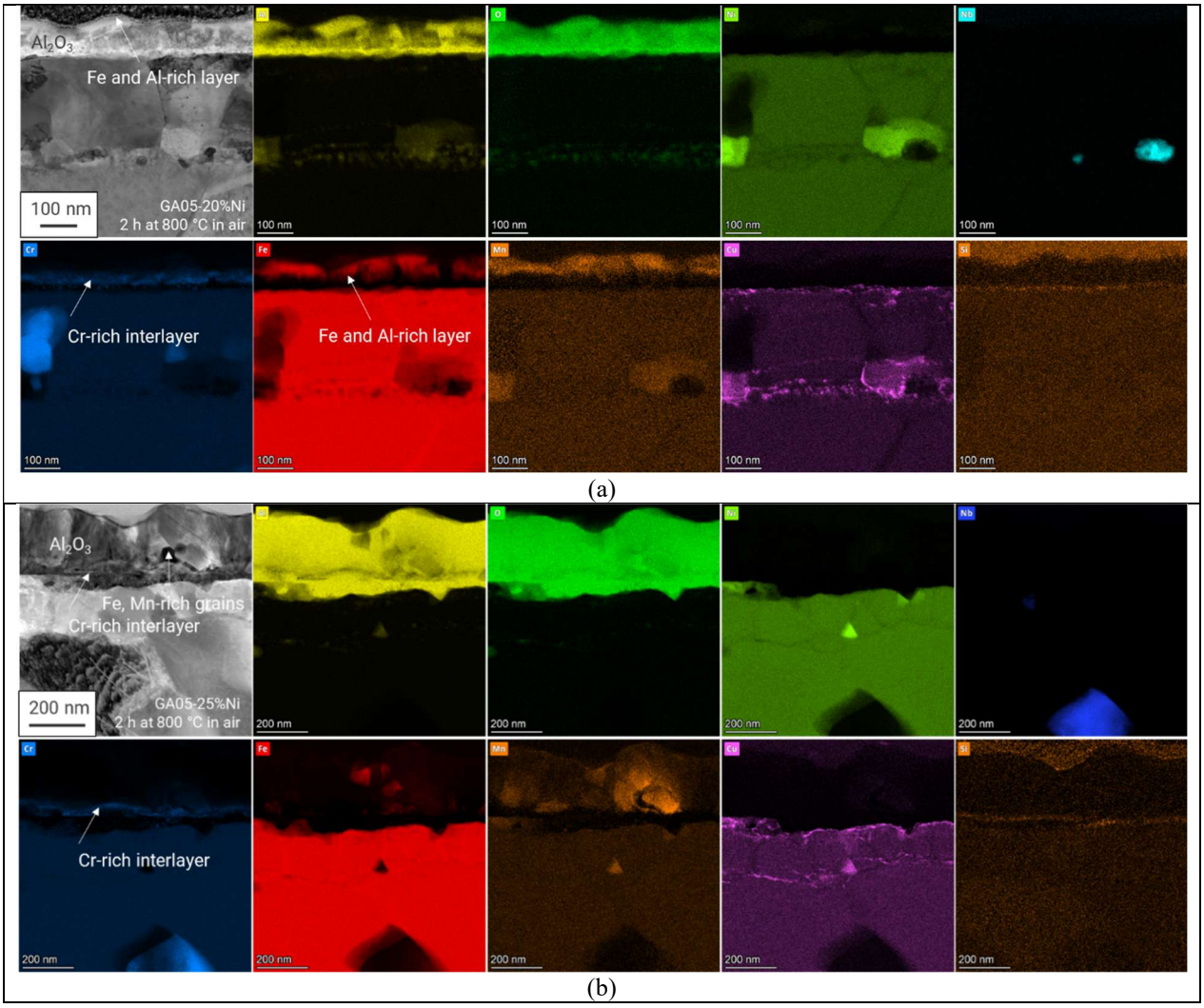

Figure 3. STEM-EDS elemental maps in wt% of pre-oxidized batch 1 (a) GA05-20Ni and (b) GA05-25Ni alloys after 2 h at 800 °C in air.

2.2 MECHANICAL PROPERTIES TESTING

Hardness of the batch 1 and batch 2 pre-oxidized specimens was measured using a Buehler VH3100 Vickers hardness indenter (Figure 4). Tests used a 1 kgf and a 15 s dwell time. Ten (10) indents were made per specimen (five per head, just above the shoulder). In one case, one specimen head was deformed by a punch press and all 10 indents were placed on the undamaged half.

For comparison, the as-solution-annealed bulk material specimens were indented with the same model instrument at Purdue University. Before pre-oxidation, the specimens were polished metallographically and indented for SEM-EBSD investigation. Twenty indents were made on each specimen under identical conditions. The GA05-20Ni specimen had an average hardness of 1.73 ± 0.15 GPa, whereas the GA05-

25Ni specimen had an average hardness of 1.87 ± 0.11 GPa. Hardness results for the batch 1 and batch 2 pre-oxidized specimens as well as the solution-annealed bulk material are given below in Figure 4.

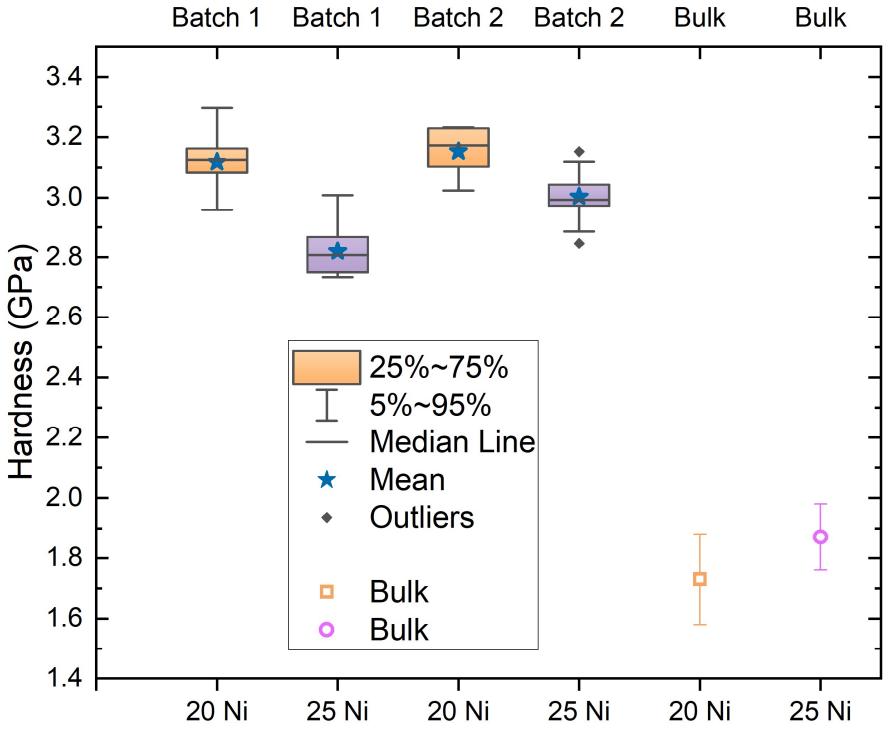

Figure 4. Hardness plots measurements on the oxidized sample surface for batch 1 (left) and batch 2 (center) and in the bulk material (right) of GA05-20Ni (orange) and GA05-25Ni (violet).

Room temperature tensile tests of GA05-20Ni and GA-05-25Ni, before and after pre-oxidation, were also conducted using SS-J3 specimens. Tensile tests were conducted on a screw-driven frame at a constant crosshead speed corresponding to a strain rate of 10^{-3}/s. Three tests were conducted for the solution-annealed and the batch 2 pre-oxidized samples, whereas only one batch 1 pre-oxidized sample was available. All individual data are plotted and compared in Figure 5.

Pre-oxidation increased yield and ultimate tensile strengths but significantly reduced ductility relative to solution-annealed samples. The strengthening is attributed to precipitation of the secondary phases during pre-oxidation at 800 °C for 2 h, including $M_{23}C_6$ (Cr-rich), MC (Nb-rich), Fe_2(Nb, Mo)-Laves phase, and NiAl-B2 phase. Similar changes in AFA stainless steels after aging are reported previously [6]. There were slight gaps in the tensile properties between the batch 1 and batch 2 pre-oxidized samples; batch 2 samples showed slightly higher yield and ultimate tensile strengths than those of batch 1. The ductility between the two batches was mostly comparable, although the batch 2 samples showed variation in both uniform and total plastic elongations. Because the solution-annealed samples also showed ductility variation similar to that of batch 2, the batch 1 samples could exhibit comparable variation with more replicates. All data will be used as the baseline properties for evaluating the effect of irradiation under liquid lead atmospheres on mechanical properties.

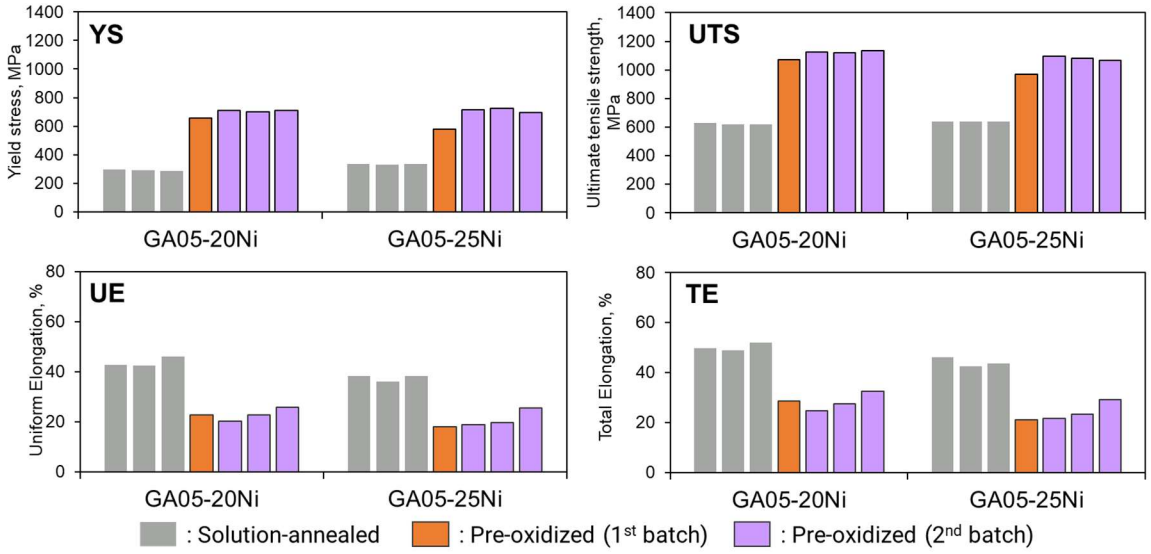

Figure 5. Room-temperature tensile properties of GA05-20Ni and -25Ni before and after pre-oxidation.

3. HFIR EXPERIMENT FABRICATION

3.1 TEST MATRIX

The BOILER irradiation experiment was previously described with the test matrix below in Table 1 [1] with batch 1 SS-J3 specimen IDs and SiC thermometer (TM) IDs added. Eight irradiation capsules, referred to as *rabbits* under the ID prefix BLR, were proposed to characterize the two alloys. For each of the two alloys, there are four rabbits—two at each design temperature of 400 and 650 °C. With three SS-J3 tensile specimens per rabbit, this provides six SS-J3 tensile specimens for each alloy/temperature combination. All eight rabbits were scheduled for irradiation in HFIR for two 23–25 day cycles to achieve a minimum of 3 dpa in the pre-oxidized AFA specimens.

Table 1. Irradiation test matrix [1]

Capsule ID	Irradiation Temperature (°C)	Alloy	Batch 1 Specimen IDs	TM IDs	Dose (dpa)	# of Cycles
BLR01	400	GA05-20Ni	G013, G014, G015	24-17, 24-18	3	2
BLR02			G004, G005, G006	24-03, 24-04		
BLR03	650		G007, G008, G009	24-05, 24-06		
BLR04			G010, G011, G012	24-07, 24-08		
BLR05	400	GA05-25Ni	G501, G502, G503	24-09, 24-10		
BLR06			G504, G505, G506	24-11, 24-12		
BLR07	650		G513, G514, G515	24-19, 24-20		
BLR08			G510, G511, G512	24-15, 24-16		

3.2 CAPSULE FABRICATION

The rabbit capsules were initially designed with 9.42 mm diameter Mo holders to passively control the rabbit temperature through an insulating radial gas gap [1]. Based on HFIR utilization at the time of part fabrication, target rod rabbit holder (TRRH) axial position 2 option was chosen. This corresponded to an insulating gas gap mixture of 71% He (Ar bal.) and 25% He (Ar bal.) to reach the 400 and 650 °C goal

temperatures, respectively [1]. Because He has a higher thermal conductivity than Ar, the mixture can be tuned to set thermal resistance across the gas gap.

For these calculations, an Al 6061 housing inner diameter of 9.52 mm was used, resulting in a nominal radial gas gap of 50 µm. However, due to part fabrication tolerances, the insulating gas gap sizes ranged from 42.5 to 47.5 µm, a reduction of up to 15%. The as-built rabbit capsule characteristics are shown in Table 2. To counteract the reduced gap size, He/Ar mixtures were adjusted, a common practice in irradiation experiments. Due to the reduction in the gas gap thermal resistance, a lower thermally conductive gas mixture is required. The as-built gas concentrations, determined later in this report, of 66% He (Ar bal.) and 20% He (Ar bal.) were selected to achieve the 400 and 650 °C goal temperatures, respectively. The updated as-built thermal analysis is provided in Section 4.

Table 2. As-built rabbit capsule gas gap information

Capsule ID	Housing Inner Diameter (mm)	Average Holder Outer Diameter (mm)	Gas Gap Size (µm)	Gap Reduction Compared to Nominal Design
BLR01	9.515	9.420	47.5	5%
BLR02	9.515	9.425	45.0	10%
BLR03	9.515	9.425	45.0	10%
BLR04	9.515	9.425	45.0	10%
BLR05	9.515	9.430	42.5	15%
BLR06	9.515	9.430	42.5	15%
BLR07	9.515	9.430	42.5	15%
BLR08	9.515	9.430	42.5	15%

The capsule parts were fabricated in accordance with the ORNL Research Reactor Division's quality assurance program. Components were engraved with unique identifiers for tracking, cleaned in acetone and ethanol (ultrasonic bath), and photographed (Appendix A). During the capsule build process, the build schematics (Appendix A) were used to track part placement.

The pre-oxidized AFA SS-J3 specimens and SiC TMs (16 x 4 mm, 0.75 mm and 0.5 mm thick, respectively) were pinned to the Mo holder bottom caps, with engraved faces aligned for tracking (Figure 6). Mo bottom end caps were then electron beam (EB) welded into the Mo holders and He leak for hermeticity.

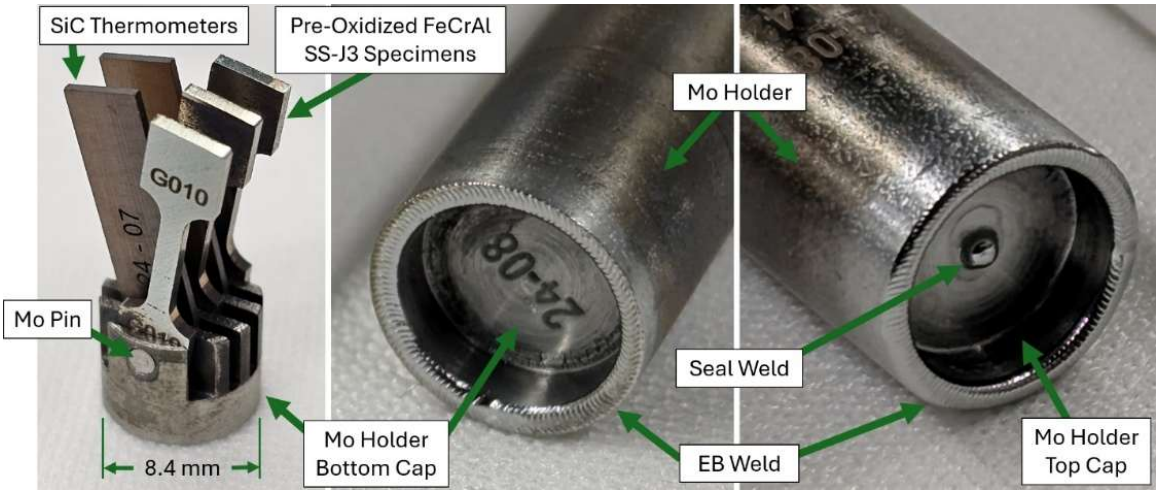

Figure 6. Capsule BLR04 holder bottom end cap assembly (left), EB weld on bottom Mo holder cap (center), and EB weld and seal weld on top Mo holder cap (right).

The partial holder assemblies were then routed for filling with 16 g high purity (99.999%) Pb slugs of 6.35 mm diameter and approximately 10 mm length. Filling was performed in an inert glovebox that was evacuated (<55 mTorr) then backfilled with He. An Al block was fabricated to heat four holder assemblies at a time on a hot plate. The block uses set screws to force the holder assembly to one side of blind holes drilled into the block. The hot plate had a setpoint temperature of 360 °C to melt Pb slugs that were lowered into the tops of the holder assemblies. A clean Mo wire was used to keep the Pb off the top welding surface. The capsules were allowed to cool before removal from the glovebox.

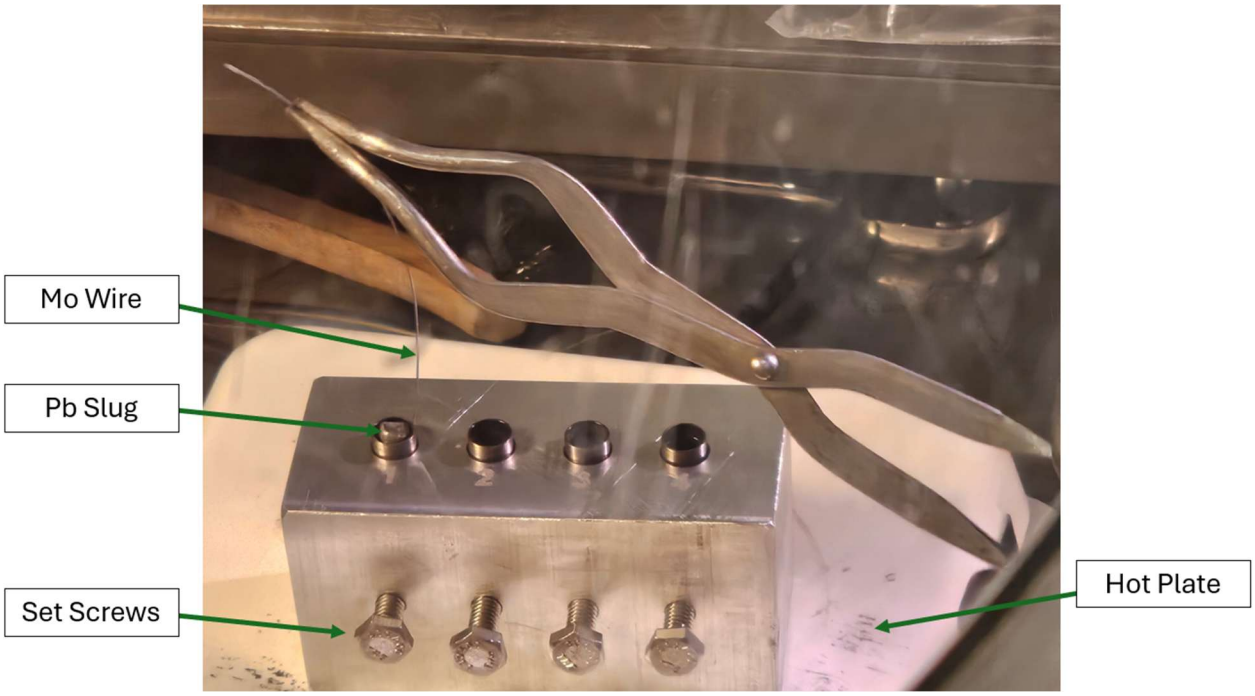

Figure 7. Capsule Pb filling setup.

The Mo top end caps were EB welded onto the partial holder assemblies. These welds were He leak checked to verify hermeticity. The assemblies were then routed to an inert glovebox that was evacuated and then backfilled with He. This operation filled the holder assemblies with He prior to a tungsten inert gas weld that was performed on a hole in the top Mo cap to seal the capsule. An example of the EB and seal welds on the top Mo cap are shown in Figure 6.

The holder assemblies were then He leak and bubble tested by ORNL non-destructive examination (NDE). Two capsules (BLR01 and BLR07) failed the leak checks and were rebuilt. The remaining six passed and were welded into Al rabbit housings and with the appropriate He/Ar gas mixture. The completed rabbits prior to delivery and insertion in HFIR are shown below in Figure 8.

Figure 8. Six Pb rabbits delivered to HFIR that began irradiation in cycle 511 (left) and two rabbits that began in cycle 512 (right).

Along with the eight rabbits destined for HFIR irradiation and two rabbits that failed NDE, two additional capsules were fabricated with the second round of assemblies described above. A total of four extra capsules were fabricated to be furnace tested to provide non-irradiated control data for comparison to the HFIR capsules. These capsules will be heated in a furnace at the temperatures determined from SiC TM dilatometry results found during post-irradiation. The four capsules are identified by the engravings on the Mo holder (rather than the visible engravings on the end caps). The four capsule IDs along with their specimen material loading are given below in Table 3. These four rabbits will not be welded into Al rabbit housings because that step is unnecessary for furnace testing. The four control capsules are stored under 5 psi He cover until furnace testing begins.

Table 3. Control rabbit capsule information

Capsule ID	Alloy	Specimen IDs	Notes
24-01	GA05-20Ni	G001, G002, G003	He Leaked at 1e-4 atm cc/s
24-09	GA05-25Ni	G507, G508, G509	He Leaked at 1e-4 atm cc/s
24-13	GA05-20Ni	G016, G017, G018	--
24-14	GA05-25Ni	G516, G517, G518	--

4. AS-BUILT CAPSULE THERMAL ANALYSIS

The experiment's thermal performance was previously modeled [1] using nominal part dimensions; however, variations due to machining tolerances resulted in a reduction in insulating gas gaps as high as 15%. To compensate, the He/Ar gas mixture were adjusted from the design values. The gas mixture of 66% He (Ar bal.) and 20% He (Ar bal.) was selected to achieve the 400 and 650 °C goal temperatures, respectively. Additionally, due to space limitations in HFIR some of the rabbits were irradiated in both TRRH axial positions 2 and 6. These two positions are considered functionally equivalent but there is a slight difference in thermal performance. The experiment was modeled using the ANSYS finite element software; updated results are given in Table 4, and temperature distributions for the specimens are given in Figure 9 and Figure 10. Inner and outer specimen values are reported separately, and Table 4 also lists combined averages for the specimen gauges.

Table 4. Estimated as-built capsule temperature results

	Component Temperature [avg (max, min)]				
	400 °C 66% He (Ar bal.)		650 °C 20% He (Ar bal.)	400 °C 66% He (Ar bal.)	650 °C 20% He (Ar bal.)
Component	**BLR01 (TRRH 2)**	**BLR02 (TRRH 6)**	**BLR03 & BLR04 (TRRH 6)**	**BLR05 & BLR06 (TRRH 2)**	**BLR07 & BLR08 (TRRH 2)**
Housing	64 (71, 55)	65 (72, 55)	65 (71, 55)	64 (71, 55)	64 (70, 55)
Housing End Cap	74 (76, 72)	72 (73, 70)	92 (93, 90)	74 (76, 72)	98 (99, 96)
Holder	336 (406, 216)	337 (408, 201)	556 (650, 368)	314 (381, 202)	520 (607, 366)
Holder Caps	313 (374, 252)	317 (401, 232)	527 (634, 419)	296 (352, 239)	494 (563, 425)
Centering Thimbles	270 (327, 213)	316 (350, 281)	478 (570, 386)	255 (307, 202)	450 (506, 393)
Lead	423 (498, 316)	430 (504, 304)	658 (732, 511)	400 (475, 296)	613 (686, 494)
Pin	362 (365, 359)	389 (393, 385)	628 (631, 626)	341 (344, 337)	558 (560, 556)
Insulator Disk	128 (265, 72)	137 (284, 76)	201 (426, 96)	123 (249, 72)	180 (377, 89)
TM	415 (470, 343)	439 (484, 368)	668 (713, 599)	392 (446, 322)	604 (658, 532)
SS-J3 (inner, gauge)	441 (453, 421)	468 (477, 451)	693 (703, 675)	418 (430, 399)	625 (639, 605)
SS-J3 (outer, gauge)	399 (419, 375)	421 (440, 398)	655 (673, 632)	375 (396, 352)	590 (610, 566)
SS-J3 (inner, tabs)	416 (476, 349)	438 (492, 374)	668 (720, 605)	393 (453, 327)	605 (664, 537)
SS-J3 (outer, tabs)	384 (441, 332)	403 (454, 354)	637 (688, 586)	361 (417, 310)	577 (635, 520)
SS-J3 (inner, shoulders)	431 (457, 391)	457 (478, 419)	684 (705, 648)	408 (433, 369)	617 (643, 578)
SS-J3 (outer, shoulders)	393 (423, 352)	414 (441, 374)	648 (675, 609)	369 (399, 330)	584 (615, 544)
SS-J3 (combined, gauge)	413 (453, 375)	437 (477, 398)	667 (703, 632)	390 (430, 352)	602 (639, 566)

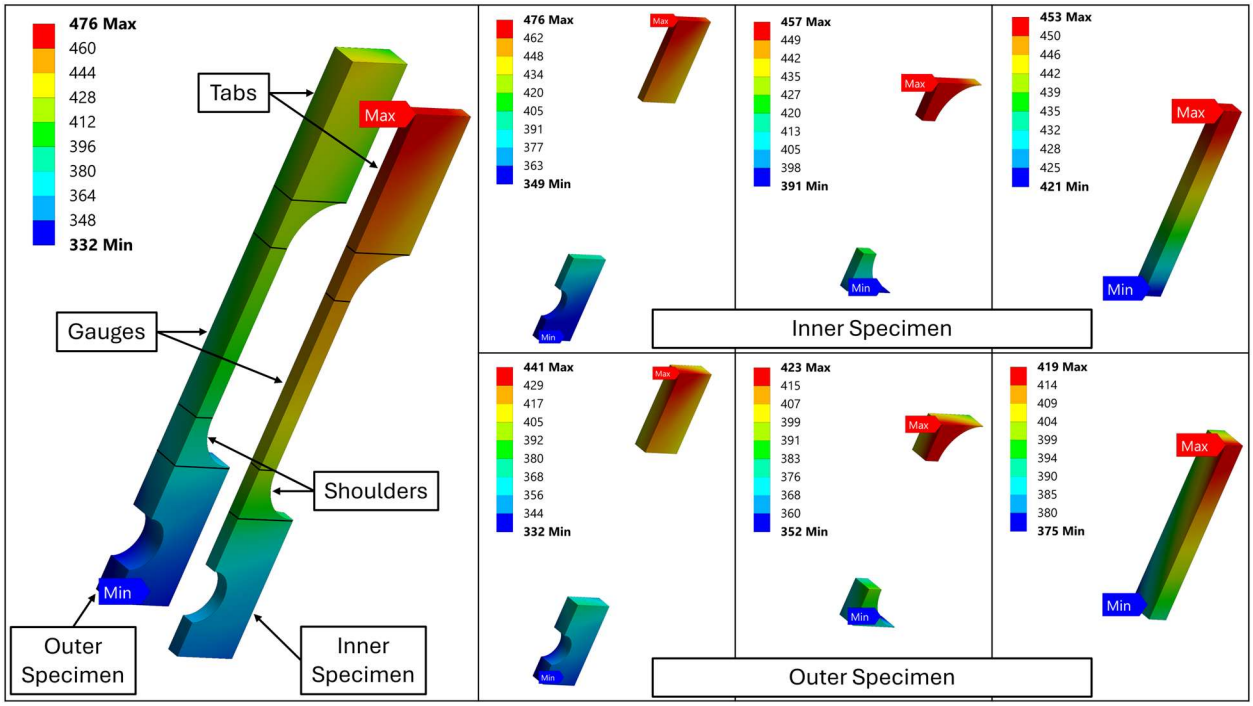

Figure 9. Predicted specimen temperature distributions (in °C) for nominally 400 °C rabbit BLR01.

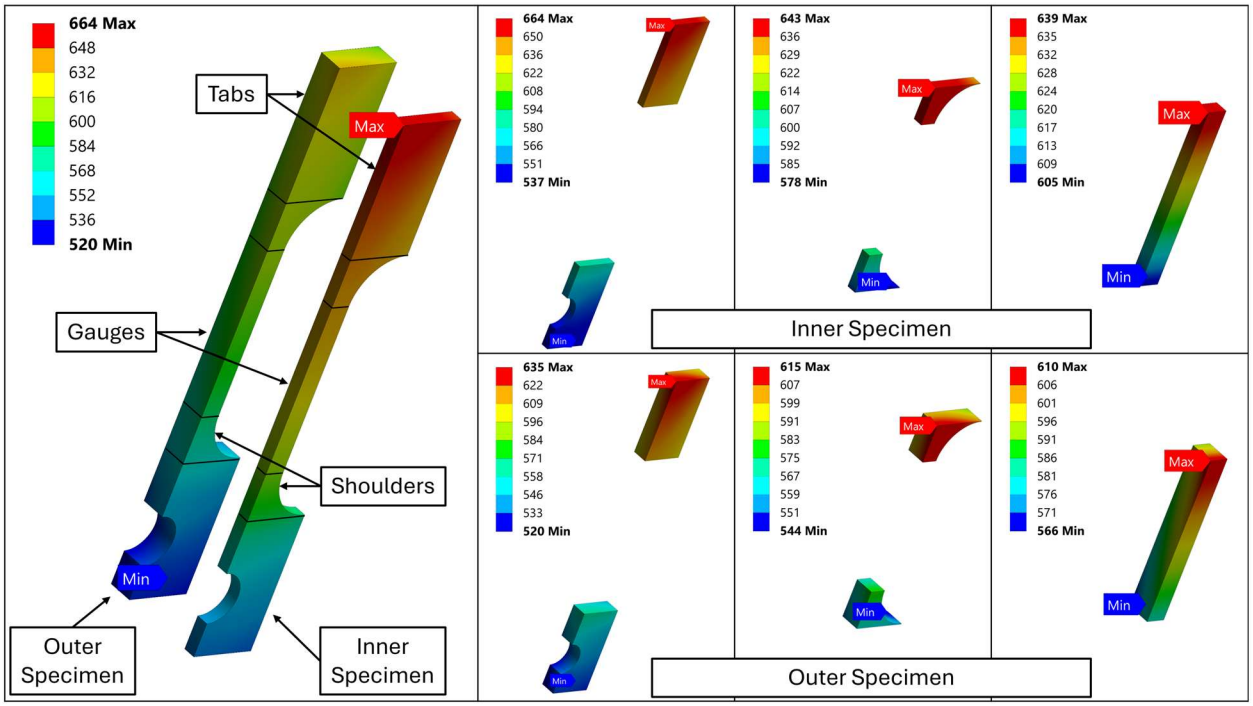

Figure 10. Predicted specimen temperature distributions (in °C) for nominally 650 °C rabbits BLR07 and BLR08.

During post-irradiation examination (PIE), the SiC TMs will be used to verify the irradiation temperature of the SS-J3 specimens. With respect to the data provided in Table 4, the average TM temperature is 1–2 °C higher than the average gauge temperature for the combined inner and outer specimens. However, compared to the individual specimens, the TM is approximately ~25 °C cooler than the inner specimen gauge and ~15 °C warmer than the outer specimen gauges.

5. IRRADIATION STATUS

The six rabbits that initially passed NDE were inserted in HFIR, beginning their two cycle irradiations in cycle 511. Cycle 511 began in February of 2025 and completed after 23.5 days. The last two rabbits that initially failed NDE were rebuilt and were installed in HFIR beginning in cycle 512. Cycle 512 is scheduled to begin in September of 2025. The first six rabbits are scheduled to complete their final irradiation cycle in cycle 512 while the last two rabbits begin their first of two cycles. The rabbit capsule loading positions in HFIR are given in Table 5. For the rabbit loading, outer ring TRRH positions were preferred due to the proximity to the HFIR fuel region for increased fast neutron flux (>0.1 MeV). Figure 11 illustrates the TRRH ring positions with respect to the fuel region. However, due to HFIR flux trap availability, mid ring and inner ring positions were utilized. Table 5 also gives the total damage accumulated, dpa, after completion of the respective cycle. Damage was estimated in the AFA specimens for both the base metal and the Al_2O_3 scale using the tool developed by Burns and Terrani [7]. Based on these calculations, the Al_2O_3 scale accumulates damage 1.8 times faster than the base AFA metal. In order to reach the 3 dpa target in the base metal, the two rabbits placed in inner ring positions will be moved to the outer ring locations vacated by earlier rabbits in this campaign. At the time of issuance of this report, cycles 512 and 513 have not completed; therefore, an estimated 24-day cycle was assumed in the damage calculations performed.

Table 5. As-built rabbit capsule irradiation positions and damage accumulation in AFA specimens

ID	Cycle 511 (23.5 days)				Cycle 512 (24 days assumed)				Cycle 513 (24 days assumed)			
	TRRH (Ring)	Axial Pos.	Damage (dpa)		TRRH (Ring)	Axial Pos.	Damage (dpa)		TRRH (Ring)	Axial Pos.	Damage (dpa)	
			Base AFA	Al_2O_3 Scale			Base AFA	Al_2O_3 Scale			Base AFA	Al_2O_3 Scale
BLR01	Delayed				D3 (Inner)	2	1.4	2.48	C6 (Outer)	2	3.22	5.78
BLR02	C2 (Mid)	6	1.65	3	C2 (Mid)	6	3.34	6.06	Removed			
BLR03	D6 (Mid)	6	1.68	3.04	D6 (Mid)	6	3.39	6.15	Removed			
BLR04	F4 (Mid)	6	1.69	3.06	F4 (Mid)	6	3.41	6.19	Removed			
BLR05	D6 (Mid)	2	1.68	3.04	D6 (Mid)	2	3.4	6.14	Removed			
BLR06	A2 (Outer)	2	1.79	3.24	A2 (Outer)	2	3.63	6.55	Removed			
BLR07	Delayed				E4 (Inner)	2	1.4	2.54	A2 (Outer)	2	3.23	5.91
BLR08	C6 (Outer)	2	1.79	3.23	C6 (Outer)	2	3.62	6.54	Removed			

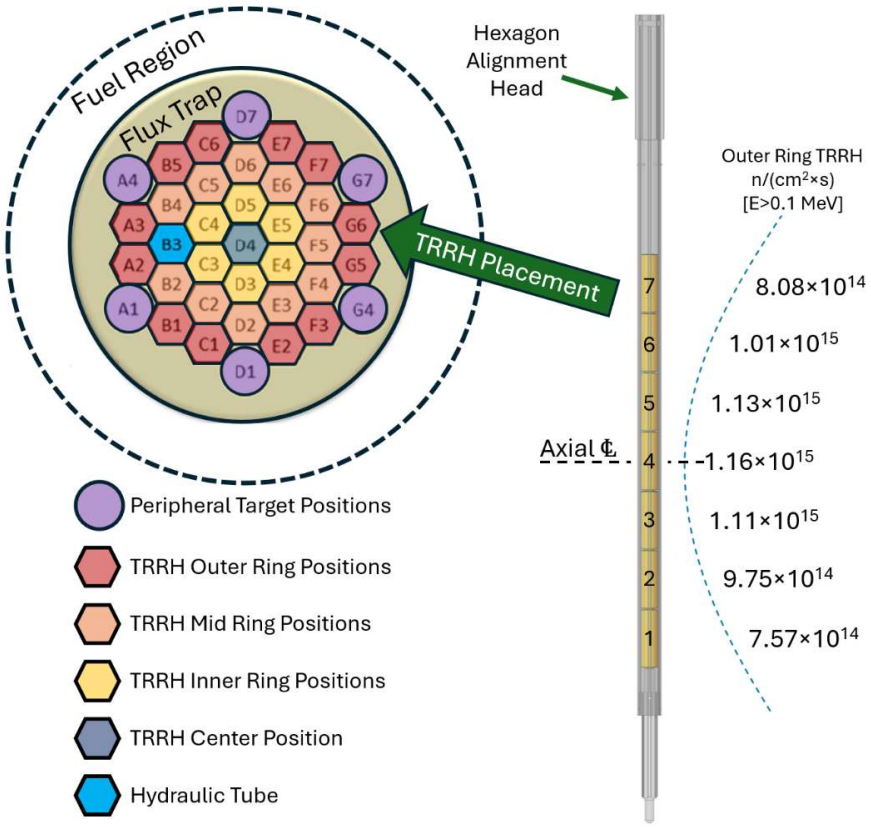

Figure 11. HFIR flux trap layout (left) and TRRH axial distribution (right).

6. POST-IRRADIATION PLAN

The rabbits will likely complete irradiation in early fiscal year 2026, depending on the completion of HFIR's next two cycles. The rabbits will be shipped to the Irradiated Material Examination and Testing (IMET) facility for disassembly. The disassembly will follow the approach used in the earlier liquid Sn HFIR experiment [8]. That process is as follows. The Al outer rabbit housing is first removed. The internal Mo holder assembly is then inverted and heated to allow the Pb to freely separate from the specimen region. The SS-J3 specimens and TMs can then be removed from the holder assembly. The specimens and TMs will likely still possess residual Pb on the surfaces that can be removed by soaking in a solution of equal parts acetic acid, ethanol, and hydrogen peroxide.

Cleaned specimens will undergo tensile testing at IMET. Fractured halves and the TMs will be sent to ORNL's Low Activation Materials Development and Analysis (LAMDA) facility. There, the specimens will undergo further microstructural characterization, and the TMs will be tested using dilatometry to verify capsule irradiation temperatures. These temperatures will then be used for the four control rabbit capsules described previously in furnace testing (reported in Table 3).

7. CONCLUSIONS

As part of the BOILER experiment under the NSUF program, two AFA steels with varying Ni concentrations, 20 wt% and 25 wt%, were developed. The specimens were oxidized prior to irradiation to grow an Al_2O_3 scale, which has been shown to limit Pb-induced dissolution [2]. Extensive pre-irradiation characterization was performed on both the solution-annealed AFA material and the Al_2O_3 scale. Higher Ni content produced thicker Al_2O_3 layers and reduced transient outer Fe- and Al-rich oxide formation. Eight irradiation rabbit capsules containing these alloys, Pb, and SiC TMs were fabricated. A thermal analysis was performed using as-built capsule dimensions to determine the fill gas concentration required to achieve the goal temperatures of 400 and 650 °C.

Although two capsules leaked during initial fabrication, the remaining six were successfully inserted in HFIR beginning in February 2025 for cycle 511. Two new capsules were fabricated, to be inserted for irradiation beginning in cycle 512. Each rabbit capsule is planned for two HFIR cycles to achieve ~3 dpa in the Fe base metal, whereas the Al_2O_3 scale is expected to reach ~6 dpa due to accelerated damage. Damage has been estimated for each rabbit based on the completed and projected cycles to confirm target levels. Two additional rabbit capsules were also assembled and paired with the previous two leaky capsules for a total of four rabbits that will be used for control furnace testing once irradiation temperatures are determined during PIE.

Finally, the initial plan for the rabbit capsule post-irradiation is described. The rabbits will be shipped to the ORNL hot cell facility for disassembly. This process, previously demonstrated in other liquid-metal irradiation experiments, provides confidence that specimens and TMs can be successfully recovered.

8. REFERENCES

[1] N. G. Russell, Y. Yamamoto, Z. Karriem, J. Salcedo Perez, K. D. Linton, T. Graening, T. G. Lach, B. A. Pint and J. P. Wharry, "NSUF BOILER Pre-Irradiation Characterization and High Flux Isotope Reactor Experiment Design," Oak Ridge National Laboratory, ORNL/TM-2024/3558, 2024.

[2] B. A. Pint and J. Jun, "Pre-Oxidation to Improve Liquid Metal Compatibility," *Oxid Met,* vol. 96, pp. 231-240, 2021.

[3] A. Chyrkin, R. Pillai, H. Ackermann, H. Hattendorf, S. Richter, W. Nowak, D. Gruner and W. J. Quadakkers, "Modeling carbide dissolution in alloy 602 CA during high temperature oxidation," *Corros. Sci.,* vol. 96, pp. 32-41, 2015.

[4] M. Romedenne, S. Dryepondt, R. Pillai, M. Lance and B. A. Pint, "High Temperature Oxidation Behavior of Fe- and Ni-Based Alloy Foils in Water Vapor at 850°C," in *Proceedings of the Corrosion 2021*, Virtual Conference, 2021.

[5] T. Galiullin, R. Pillai, W. J. Quadakkers and D. Naumenko, "MAR-M-509, Differences in Oxidation Behavior of Conventionally Cast and Additively Manufactured Co-Base Alloy," *High Temperature Corrosion of Materials,* vol. 100, pp. 791-816, 2023.

[6] H. Bei, Y. Yamamoto, M. P. Brady and M. L. Santella, "Aging effects on the mechanical properties of alumina-forming austenitic stainless steels," *Materials Science and Engineering: A,* vol. 527, no. 7-8, pp. 2079-2086, 2010.

[7] J. R. Burns and K. A. Terrani, "A Web-Based Application for Standardization of Radiation Damage Calculations," in *Transactions of the American Nuclear Society, Vol. 119, pg 416-418*, Orlando, FL, 2018.

[8] M. Kondo, B. A. Pint, J. Jun, N. G. Russell, J. L. McDuffee, M. Akiyoshi, T. Tanaka, N. Oono, J. Miyazawa, J. W. Geringer, Y. Kato and Y. Hatano, "Conceptual design of HFIR irradiation experiment for material compatibility study on liquid Sn divertor," *Plasma Fusion Res.,* vol. 16, no. 2405040, 2021.

APPENDIX A. AS-BUILT RABBIT CAPSULE PICTURES AND SUPORTING GRAPHICS

Figure 12. Capsule BLR01 part layout.

Figure 13. Capsule BLR02 part layout.

Figure 14. Capsule BLR03 part layout.

Figure 15. Capsule BLR04 part layout.

Figure 16. Capsule BLR05 part layout.

Figure 17. Capsule BLR06 part layout.

Figure 18. Capsule BLR07 part layout.

Figure 19. Capsule BLR08 part layout.

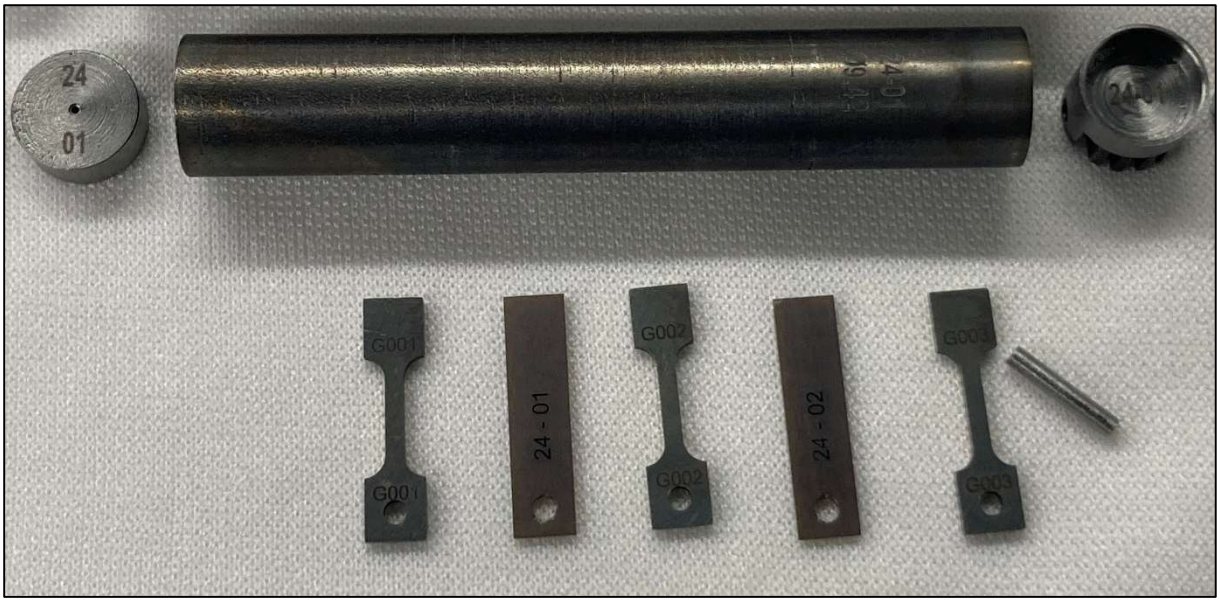

Figure 20. Furnace test capsule 24-01 part layout.

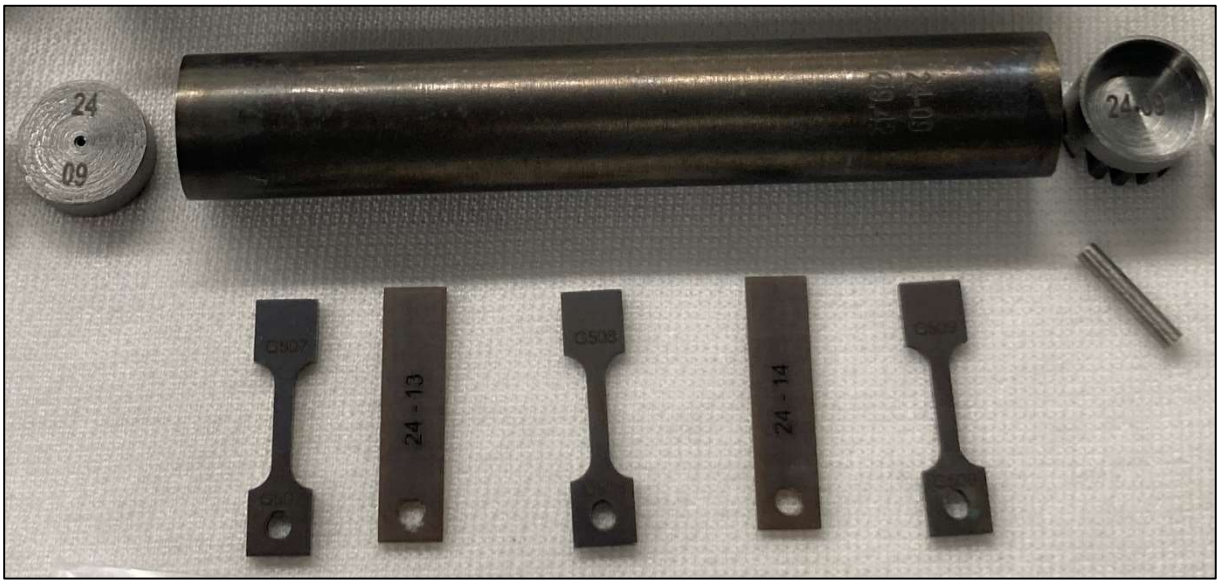

Figure 21. Furnace test capsule 24-09 part layout.

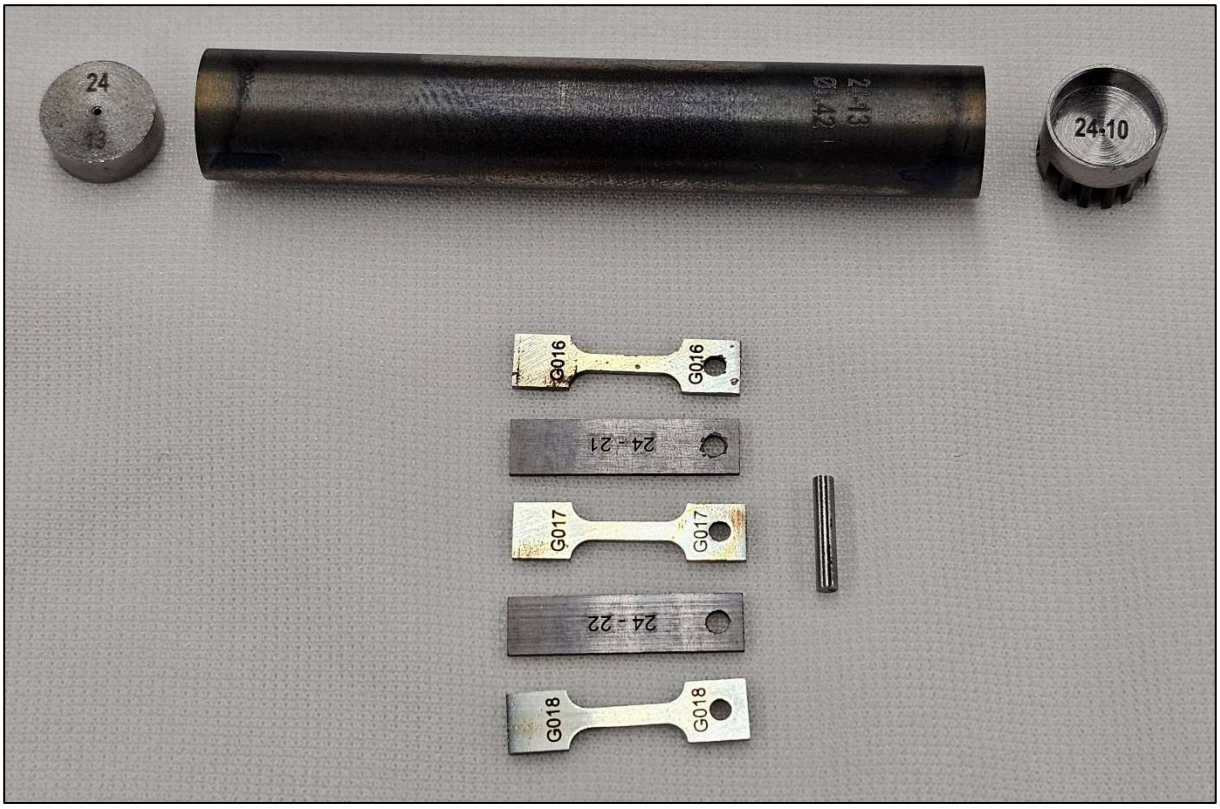

Figure 22. Furnace test capsule 24-13 part layout.

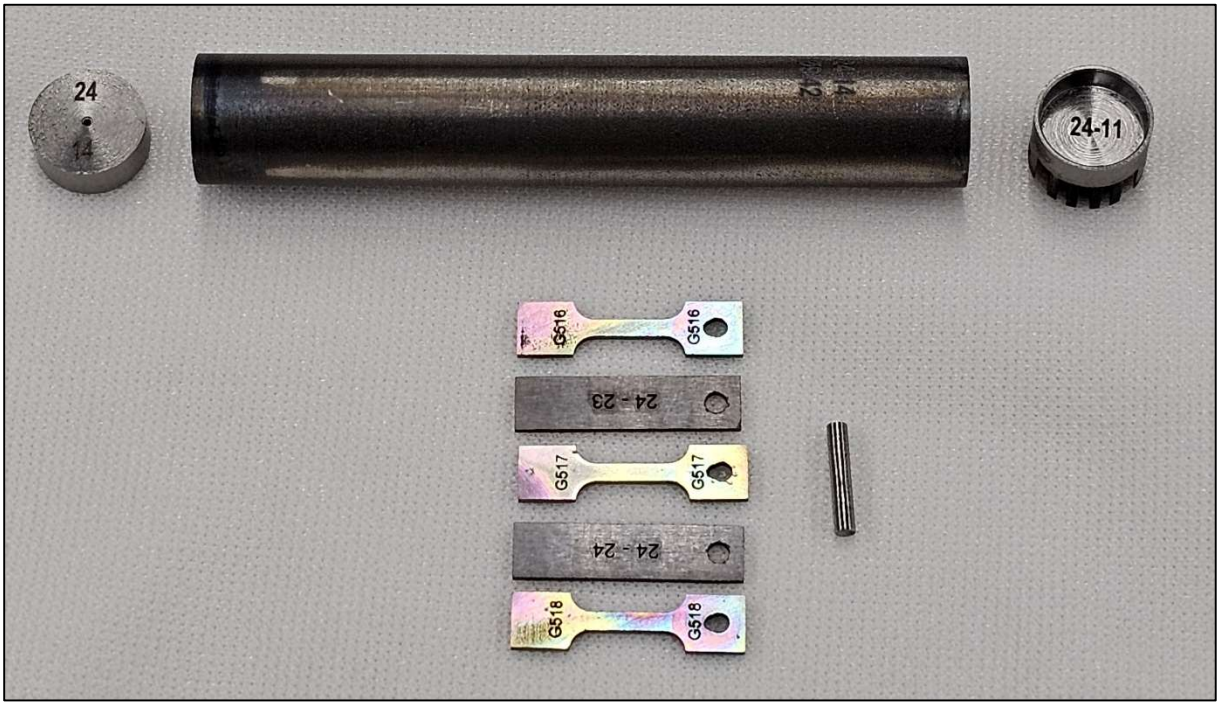

Figure 23. Furnace test capsule 24-14 part layout.

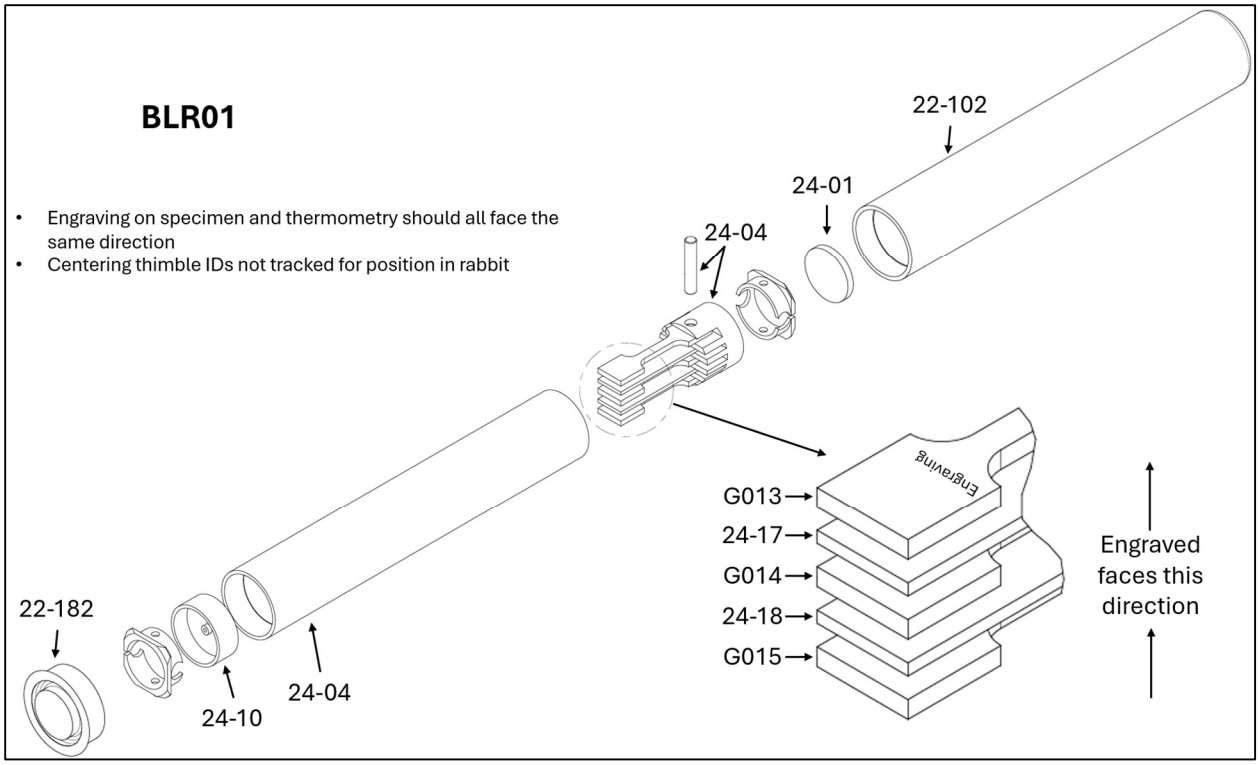

Figure 24. Capsule BLR01 build schematic.

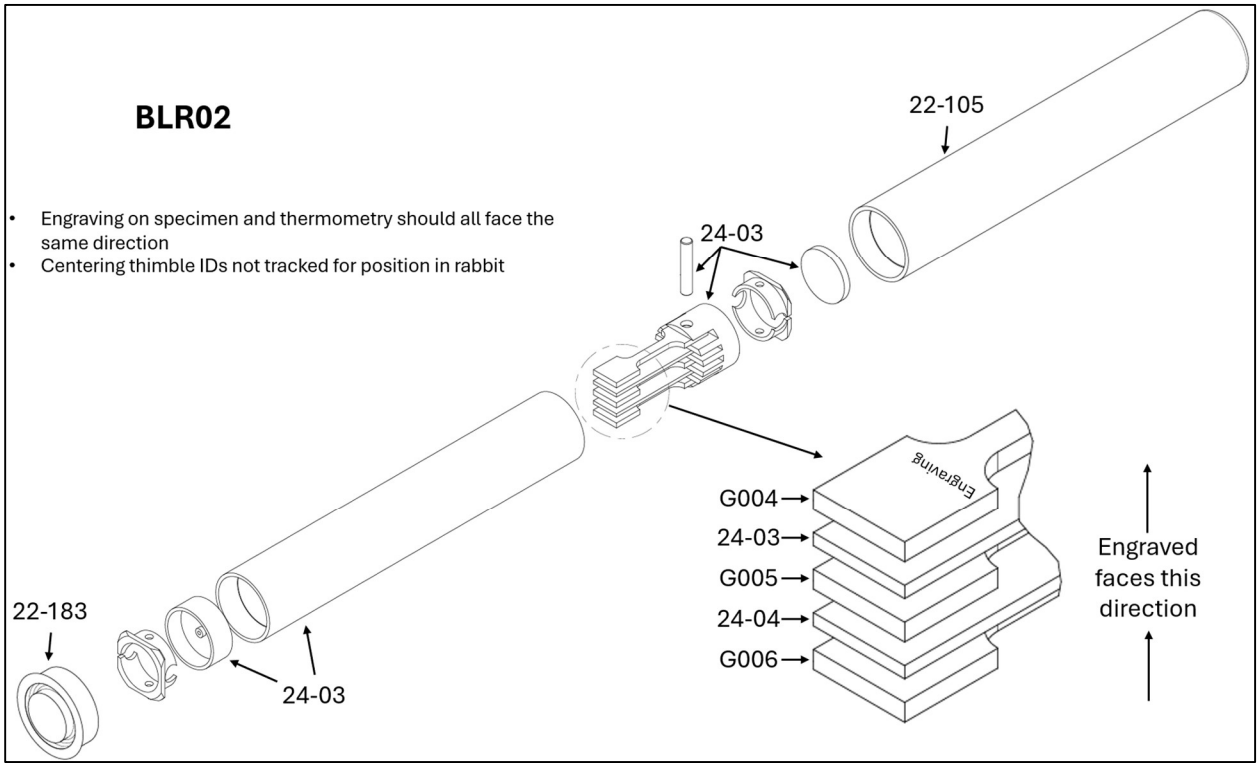

Figure 25. Capsule BLR02 build schematic.

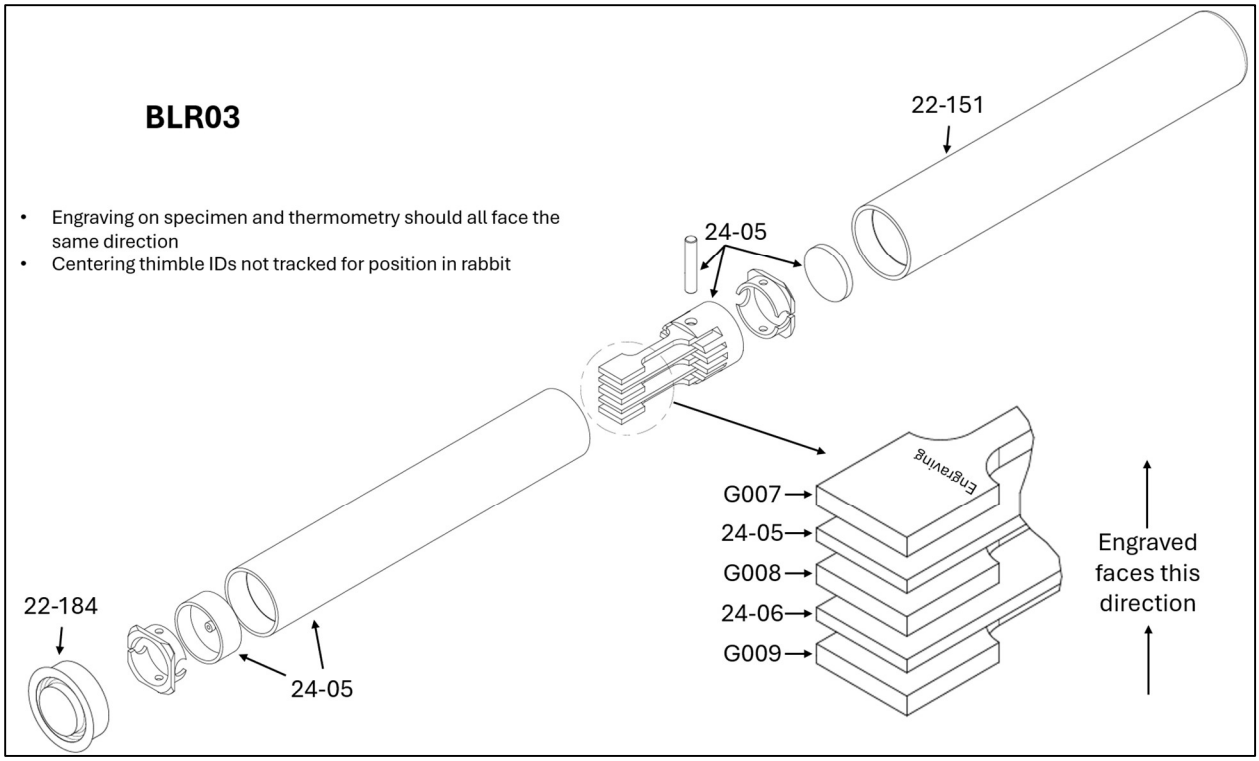

Figure 26. Capsule BLR03 build schematic.

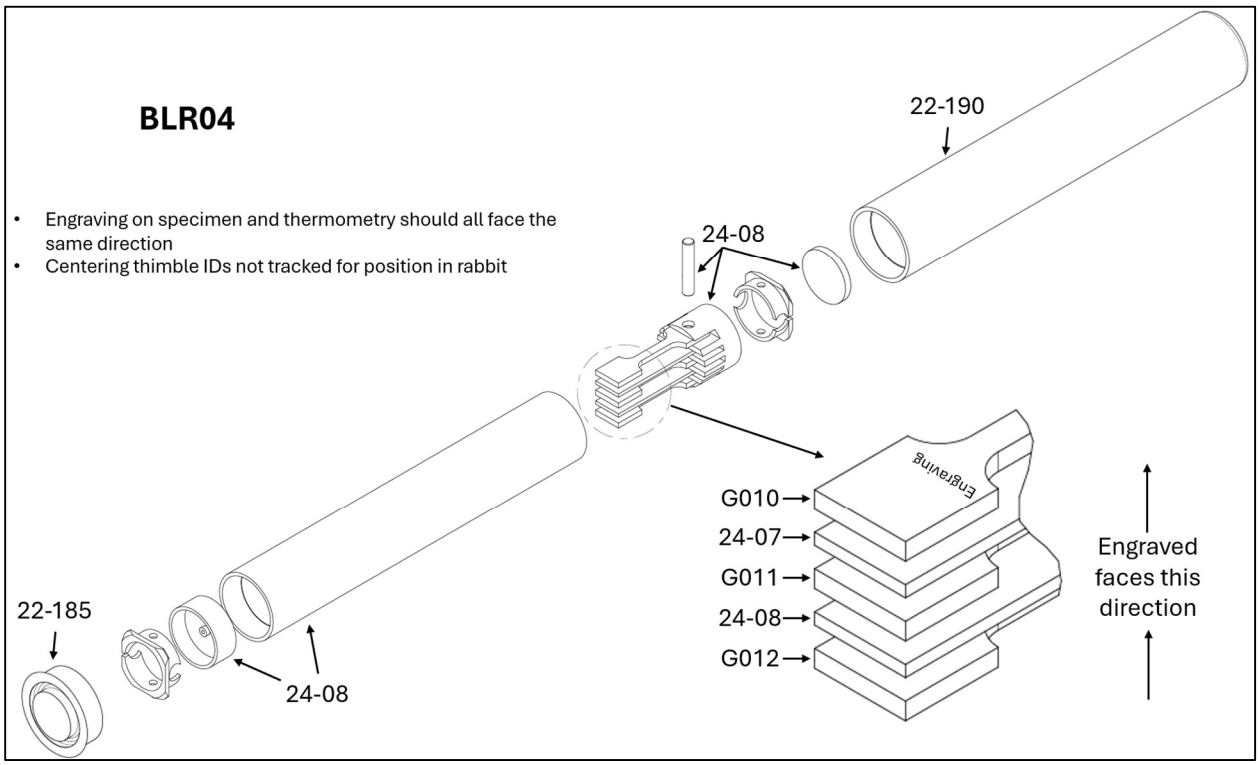

Figure 27. Capsule BLR04 build schematic.

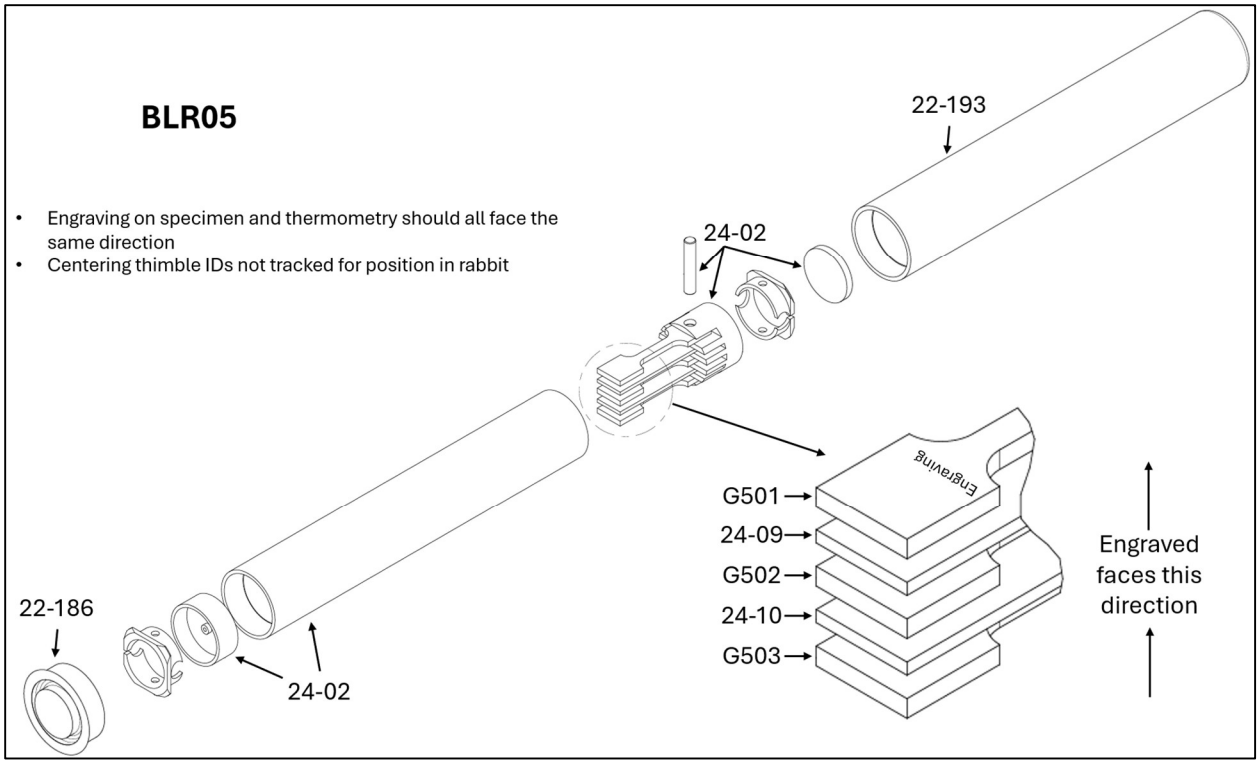

Figure 28. Capsule BLR05 build schematic.

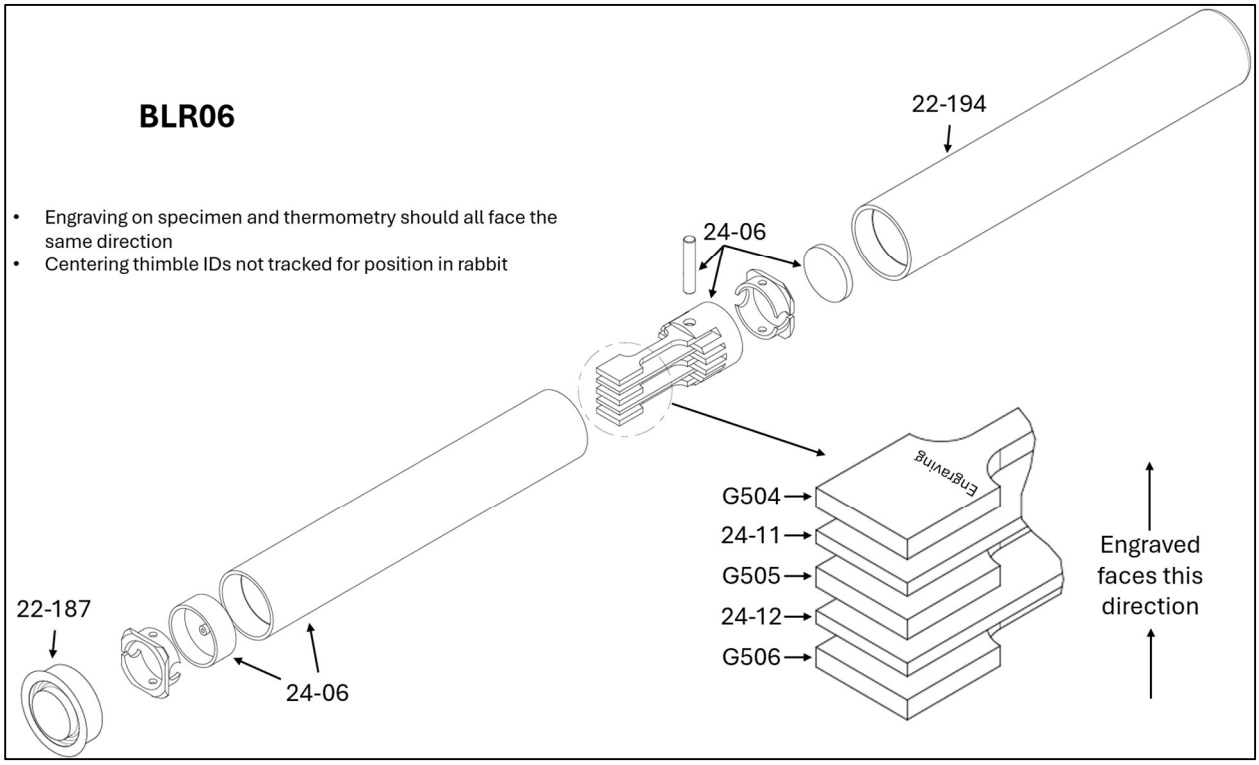

Figure 29. Capsule BLR06 build schematic.

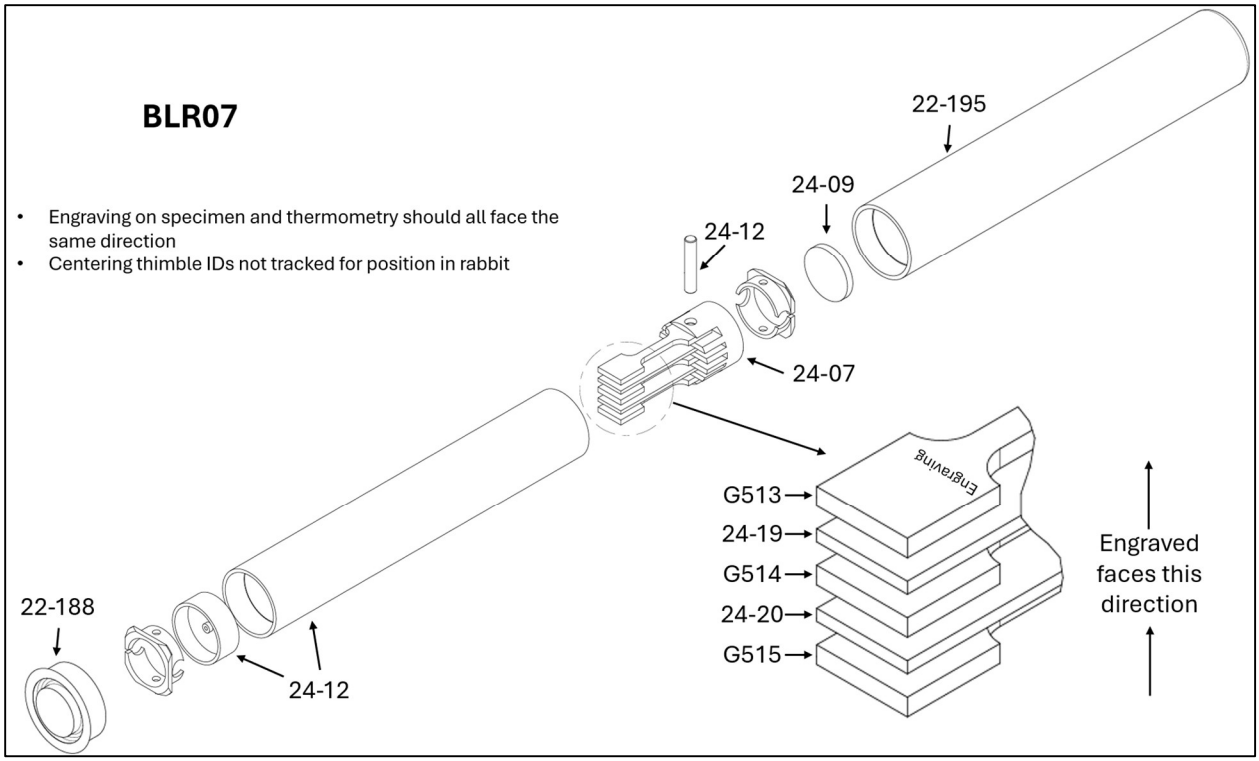

Figure 30. Capsule BLR07 build schematic.

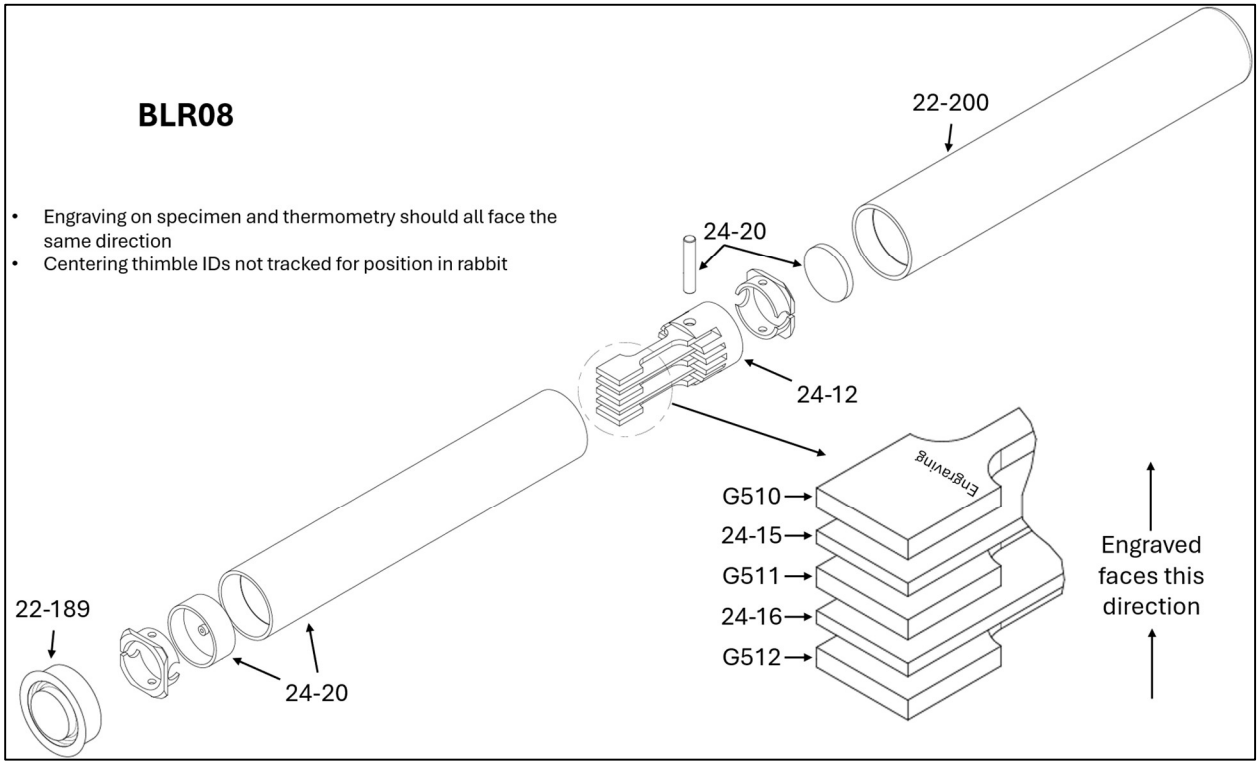

Figure 31. Capsule BLR08 build schematic.

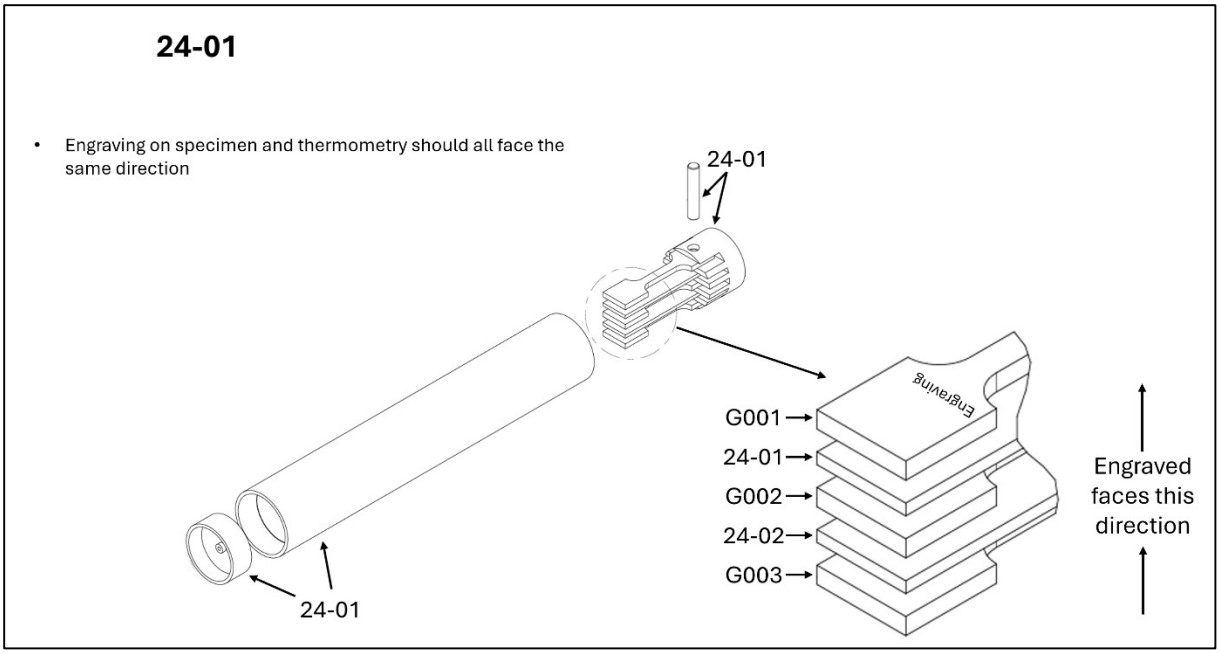

Figure 32. Furnace test capsule 24-01 build schematic.

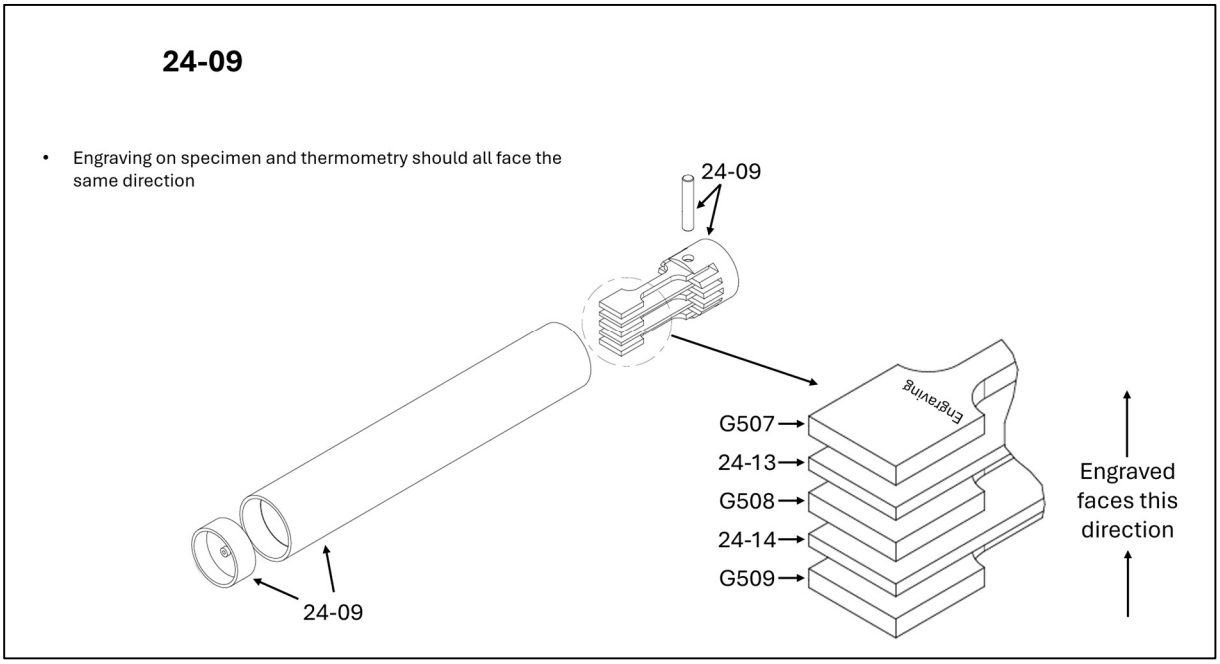

Figure 33. Furnace test capsule 24-09 build schematic.

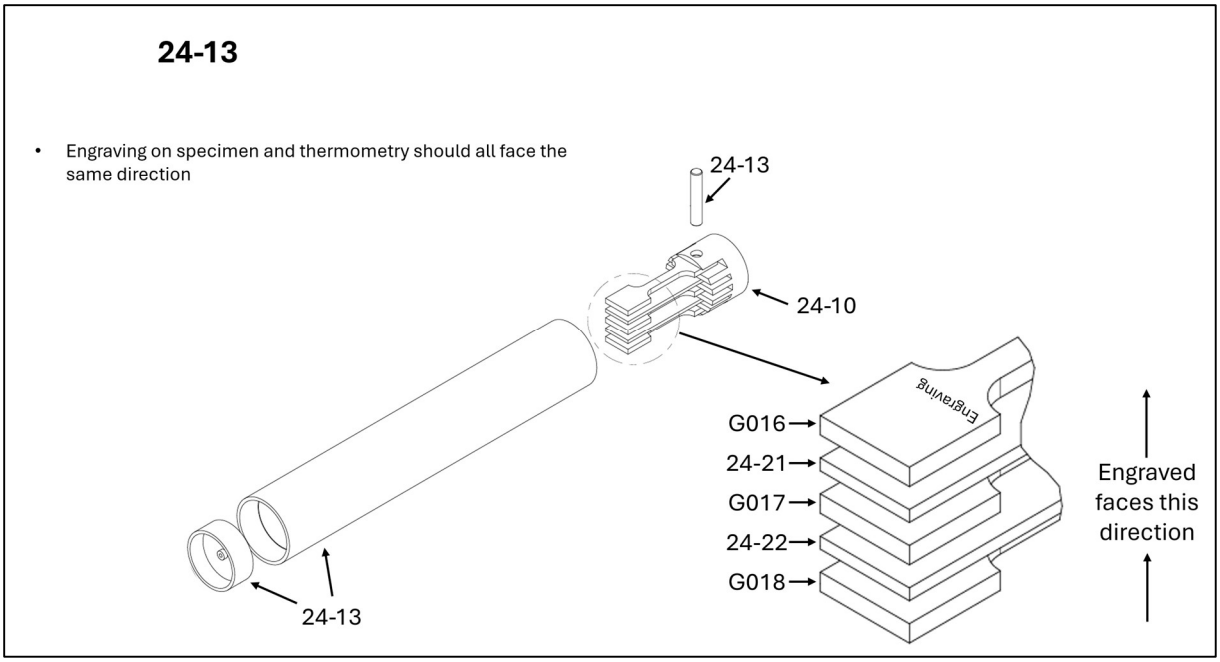

Figure 34. Furnace test capsule 24-13 build schematic.

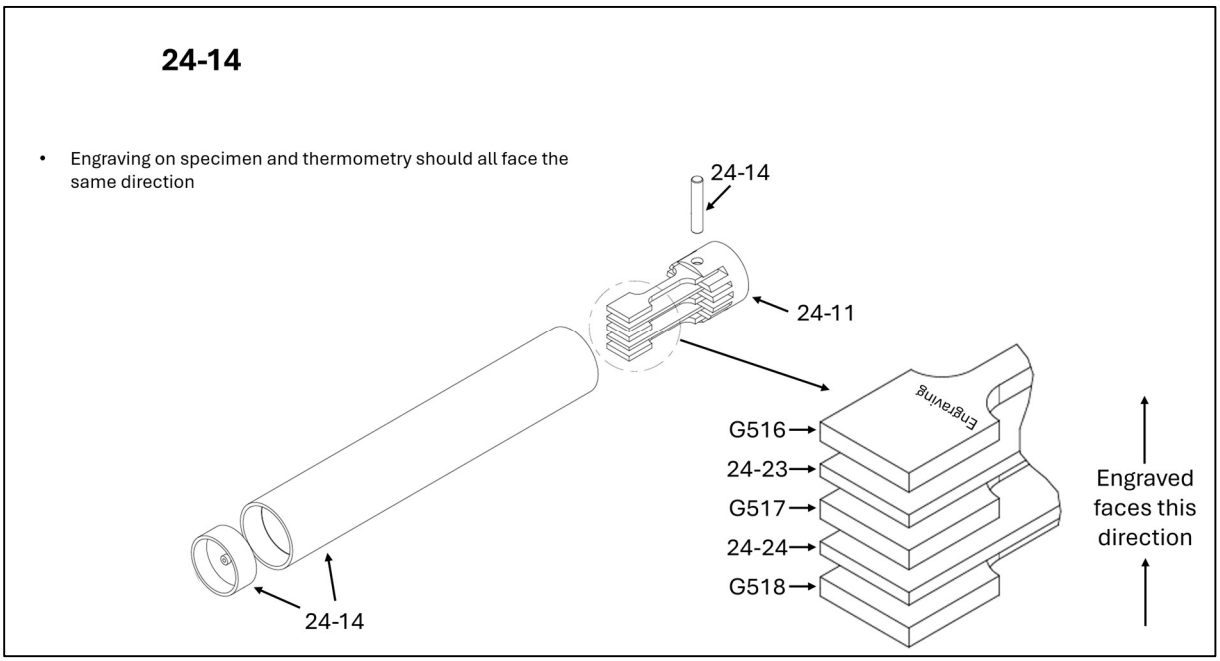

Figure 35. Furnace test capsule 24-14 build schematic.